iScience

Article

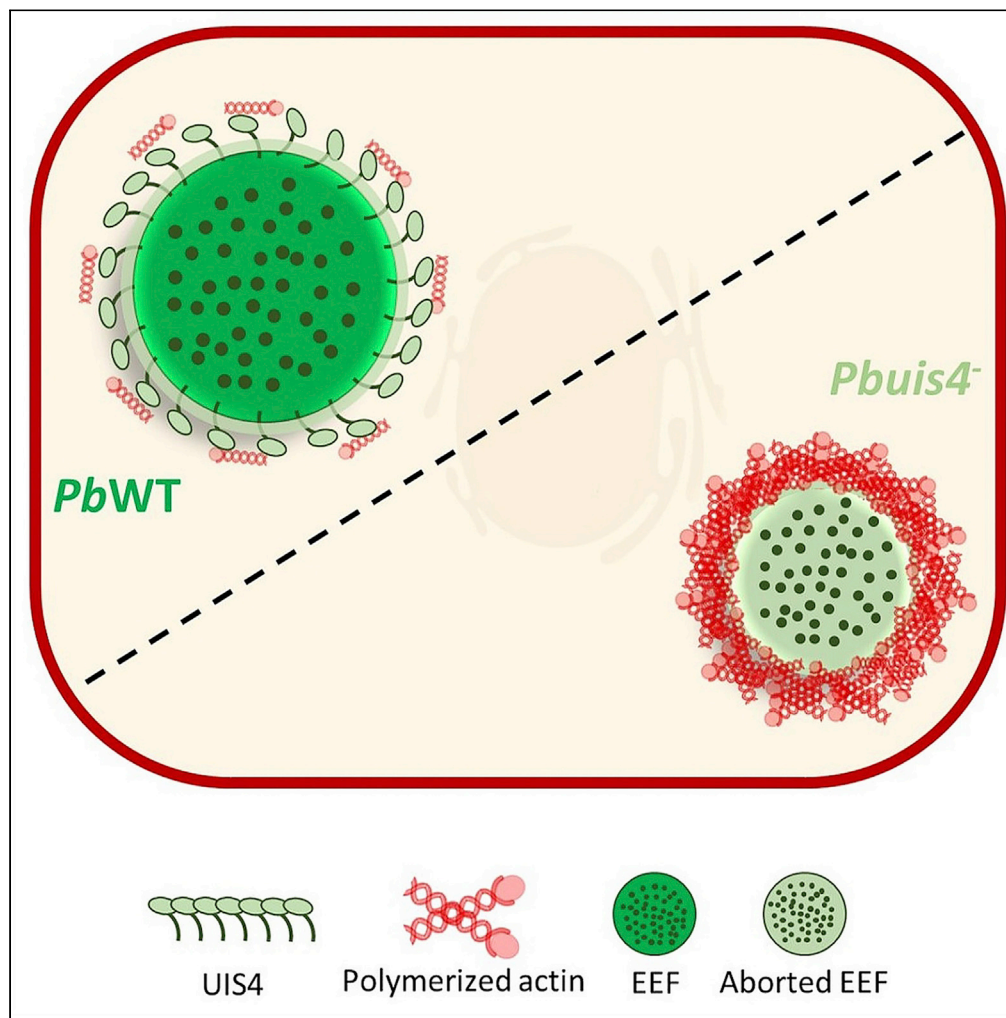# *Plasmodium* parasitophorous vacuole membrane-resident protein UIS4 manipulates host cell actin to avoid parasite elimination

Viriato M'Bana,
Aparajita Lahree,
Sofia Marques,
Ksenija Slavic,
Maria M. Mota

mmota@medicina.ulisboa.pt

Highlights

Plasmodium PVM-resident protein UIS4 interacts with host cell actin

Host actin dynamics is altered around exoerythocytic forms (EEFs) lacking UIS4

Actin activity around EEFs lacking UIS4 is associated with parasite elimination

Parasite elimination depends on actomyosin complexes formed around the PVM

Article

Plasmodium parasitophorous vacuole membrane-resident protein UIS4 manipulates host cell actin to avoid parasite elimination

Viriato M'Bana,[1,2] Aparajita Lahree,[1] Sofia Marques,[1] Ksenija Slavic,[1] and Maria M. Mota[1,3,*]

SUMMARY

Parasite-derived PVM-resident proteins are critical for complete parasite development inside hepatocytes, although the function of most of these proteins remains unknown. Here, we show that the upregulated in infectious sporozoites 4 (UIS4) protein, resident at the PVM, interacts with the host cell actin. By suppressing filamentous actin formation, UIS4 avoids parasite elimination. Host cell actin dynamics increases around UIS4-deficient parasites, which is associated with subsequent parasite elimination. Notably, parasite elimination is impaired significantly by the inhibition of host myosin-II, possibly through relieving the compression generated by actomyosin complexes at the host-parasite interface. Together, these data reveal that UIS4 has a critical role in the evasion of host defensive mechanisms, enabling hence EEF survival and development.

INTRODUCTION

Plasmodium parasites cause malaria, a disease which still kills a child every 2 min (World Health Organization, 2020). The infection of the mammalian host is initiated with the hepatotropic forms of the parasite, called sporozoites, which are injected into the host's skin through the bite of an infected female *Anopheles* mosquito. Sporozoites migrate to the liver where they invade hepatocytes (Prudêncio et al., 2006). The efficient intra-hepatic residency and maturation of *Plasmodium* parasites requires the establishment of a specialized membrane-bound compartment called the parasitophorous vacuole (PV), which physically separates the parasite from the host cell cytoplasm. Though the PV membrane (PVM) remains poorly characterized, it is known that the PVM and its resident proteins play critical roles for the benefit of the parasite (Hanson et al., 2013), ranging from protection to signaling and waste elimination (Liehl et al., 2015; Spielmann et al., 2012). Indeed, parasites deficient in some of the PVM-resident proteins have been shown to fail in development or are efficiently eliminated at different stages during development (Mueller et al., 2005; Real et al., 2017; Sá e Cunha et al., 2017). However, the molecular understanding of the interactions occurring at this interface and the roles of the different PVM resident proteins in this regard remain poorly studied. Such is the case of the upregulated in infective sporozoites 4 protein (UIS4) (Kaiser et al., 2004). Sporozoites of the rodent malaria species—*P. berghei* and *P. yoelii*—lacking UIS4 are capable of hepatocytes invasion and of initiating replication but are unable to efficiently complete their developmental program. The vast majority of *uis4⁻* parasites are eliminated and the few breakthroughs fail to reach the advanced developmental stages as their wild-type parasites counterparts (Mueller et al., 2005). Previous studies have indicated a reduction in the recruitment of lysosomes to the region surrounding the PVM during *P. berghei* development in the liver for UIS4-deficient parasites (Petersen et al., 2017). Despite its imminent role in the successful completion of the liver stage of infection, the biological function of UIS4 remains unclear. The present study describes the role of the UIS4 protein during the liver stages of *P. berghei* wherein it aids parasite survival by eluding host actin structures deployed as part of host cytosolic defense.

RESULTS

P. berghei UIS4 interacts with host cell actin

P. berghei uis4⁻ (*Pbuis4⁻*) parasite line was generated in the *P. berghei* ANKA background and followed over liver-stage development to recapitulate previous published results (Mueller et al., 2005) (Figures 1A–1C and S1A–S1H). As an interface between the parasite and its host, the PVM is expected to mediate the first line of interactions between these two entities. Hence, we sought to assess the role of *Pb*UIS4 by employing immunoprecipitation to screen for its putative interacting partners. Anti-*Pb*UIS4

[1]Instituto de Medicina Molecular João Lobo Antunes, Faculdade de Medicina da Universidade de Lisboa, 1649-028 Lisboa, Portugal

[2]Pós-graduação Ciência para o Desenvolvimento, Portugal

[3]Lead contact

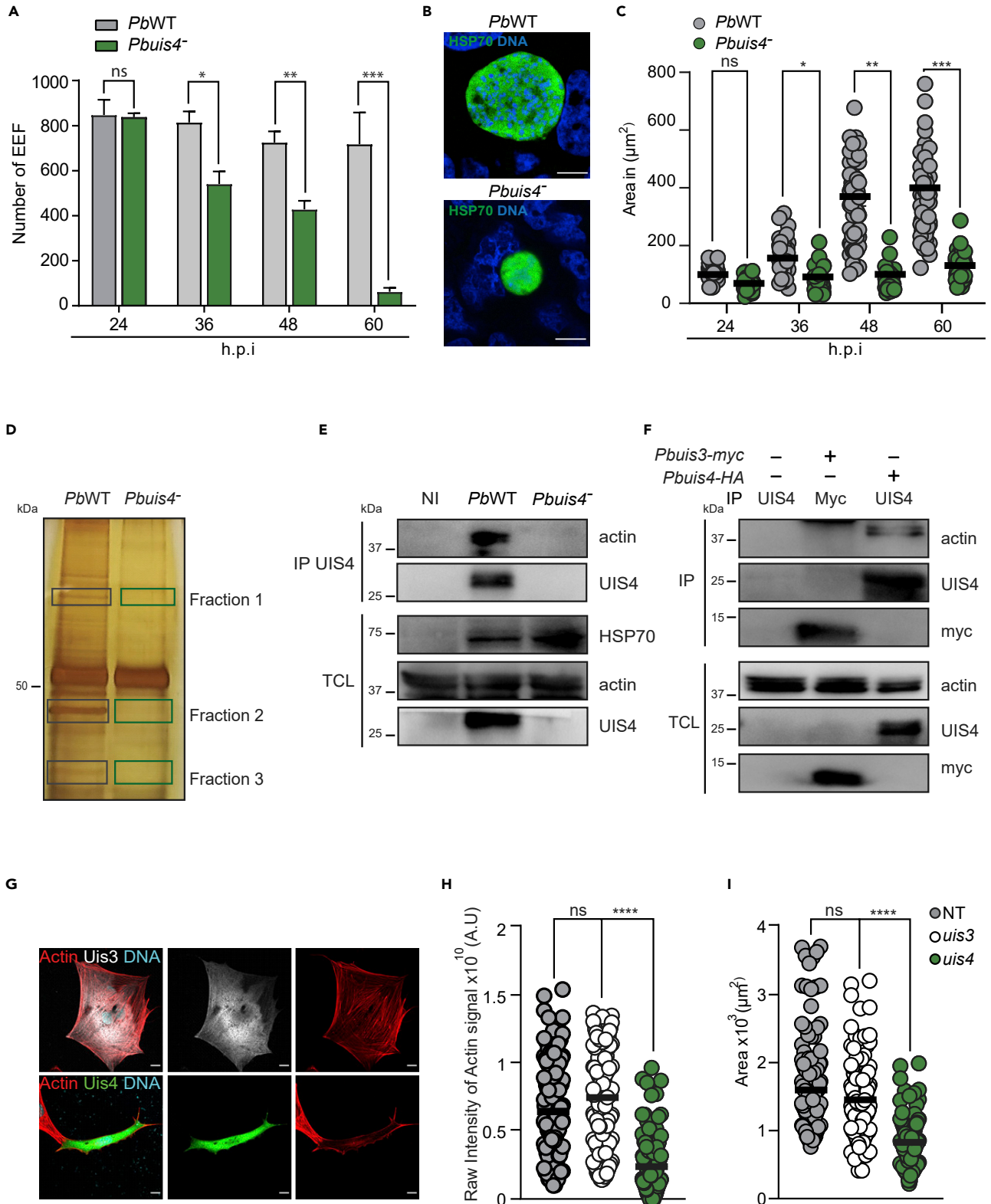*Correspondence: mmota@medicina.ulisboa.pt

Figure 1. *P. berghei* UIS4 interacts with and manipulates host cell actin

(A, B, and C) Huh7 cells were infected with *Pb*WT (gray bars or symbols) or *Pbuis4*⁻ (green bars or symbols) parasites, fixed at indicated time points and immunostained with anti-*Pb*HSP70 and Hoechst (N = 3). A number of exoerythrocytic forms (EEFs) from 24 h.p.i to 60 h.p.i.; (B) Representative micrographs of analyzed EEFs at 60 h.p.i (*Pb*HSP70-green, DNA dye Hoechst-blue, scale bar: 10 μm).

(C) EEF size from 24 h.p.i to 60 h.p.i. measured as EEF area (each symbol represents one EEF, about 150 EEFs analyzed per experiment).

(D) Huh7 cells were infected with either *Pb*WT or *Pbuis4*⁻ parasites, lysed at 24 h.p.i. and immunoprecipitated with anti-*Pb*UIS4. Immunoprecipitated proteins were resolved by SDS-PAGE followed by silver staining. Gray and green boxes indicate the regions excised for subsequent mass-spectrometric analysis.

(E) Huh7 cells were either infected with *Pb*WT or *Pbuis4*⁻ parasites or maintained as non-infected controls (NI). Cells were lysed at 24 h.p.i. and lysates immunoprecipitated with anti-*Pb*UIS4. Immunoprecipitated proteins were probed for Western Blot analysis with anti-actin (top panel) and anti-*Pb*UIS4 (middle panel). Total cell lysates (TLC, bottom panels) were probed with anti-actin, anti-*Pb*HSP70, and anti-*Pb*UIS4.

(F) HEK 293-T cells were maintained as non-transfected controls (NT) or transfected with plasmids expressing the cytosolic domains of either *Pbuis3-myc* (*uis3*) or *Pbuis4*-HA (*uis4*). Cells were lysed at 48 h after transfection and immunoprecipitated with anti-myc or anti-*Pb*UIS4, respectively. Immunoprecipitated proteins (top panels) and TCL (bottom panels) were probed with anti-actin, anti-myc (to detect UIS3-myc), and anti-*Pb*UIS4.

(G, H, and I) 3T3 fibroblasts were transfected with either *Pbuis3-myc*- or *Pbuis4*-expressing plasmids and seeded on coverslips. Cells were fixed at 48 h after transfection and immunostained with anti-myc antibody (to detect UIS3-myc), anti-UIS4 antibody, and Phalloidin (actin binding dye) (N = 3 with 50 cells analyzed in average per condition and per experiment).

(G) Representative images of actin signal (red) for intensity quantification and cell size evaluation (UIS4-green, UIS3-white, and DNA-blue, scale bar: 10 μm);

(H) Quantification of total (raw) actin signal intensity in transfected (white and green symbols) and non-transfected (NT, gray) cells.

(I) Area of non-transfected cells (gray) and cells transfected with either *Pbuis3-myc*- (white) or *Pbuis4*-expressing plasmids (green). Data in (A) are represented as mean ± SE of mean (SEM), data in (C, H, and I) represented as individual data points, with a black line representing the mean. Statistical analysis of means was performed using two-tailed Mann-Whitney U test, ns represents p > 0.05; *p < 0.05; **p < 0.01; ***p < 0.005 and ****p < 0.001.

(A) n = 1695 (24 h.p.i, *Pb*WT), 1629 (36 h.p.i, *Pb*WT), 1451, (48 h.p.i, *Pb*WT), 1436 (60 h.p.i, *Pb*WT), 1675 (24 h.p.i, *Pbuis4*⁻), 1082 (36 h.p.i, *Pbuis4*⁻), 856 (248 h.p.i, *Pbuis4*⁻) and 125 (60 h.p.i, *Pbuis4*⁻) EEFs counted in two independent experiments.

(C) n = 150 EEFs counted per time point in two independent experiments.

(I and J) n = 170 (NT), 130 (*uis3* transfected), and 150 (*uis4* transfected) cells quantified in 3 independent experiments. See also Figures S1 and S2 and Table S1.

antibody (Thieleke-Matos et al., 2016) was used to probe the lysates of the hepatoma cell line Huh7, infected either with *Pb*WT or *Pbuis4*⁻ parasites (Figures S1C–S1E). Immunoprecipitation was carried out at 24 h post-infection (h.p.i), where the number and size of *Pb*WT and *Pbuis4*⁻ exoerythrocytic forms (EEFs) was similar (Figures 1A–1C). The immunoprecipitated proteins were resolved by SDS-PAGE and visualized by silver staining, to infer the purity as well as the abundance and diversity of proteins in these samples. The immunoprecipitated samples obtained from cells infected with *Pb*WT parasites showed a greater variety of proteins than those derived from *Pbuis4*⁻-infected cells (Figure 1D). Three differential bands were detected, excised, and analyzed by mass spectrometry (Figure 1D – highlighted by the gray boxes). The regions corresponding to the molecular weights of those bands in the lane of immunoprecipitated proteins obtained from *Pbuis4*⁻ infected cells were also excised and analyzed as controls (Figure 1D - highlighted by the green boxes). The mass spectrometric (MS) analysis detected several putative candidates with the highest score assigned to a 41 kDa protein in Fraction 2 of the *Pb*WT sample, which was identified as actin (protein score of 755 and sequence coverage of 62%, Table S1). Notably, the analysis of *Pbuis4*⁻ control fractions did not identify any protein (Table S1, for data robustness, a lower threshold score of 70 was considered for protein identification). To validate actin (ACTG_HUMAN - Actin), the top candidate from the MS dataset, as a UIS4 interactor, proteins co-immunoprecipitated with anti-*Pb*UIS4 were immunoblotted using an anti-actin antibody, which confirmed the presence of actin within the proteins co-precipitated with *Pb*UIS4 (Figures 1E and S2A). Furthermore, we could also detect a mild signal of host actin in proximity to the PVM of young schizonts in infected hepatocytes (Figure S1I).

*Pb*UIS4 is predicted to possess a domain facing the PV (a space between the parasite plasma membrane and the PVM), one transmembrane domain implanted in the PVM, and a cytosolic domain facing the host cell cytosol (Madeira et al., 2019). Thus, we hypothesized that *Pb*UIS4 interacts with the host actin via its cytosolic domain. To test this hypothesis, we carried out immunoprecipitation experiments using human embryonic kidney cells (HEK 293-T) expressing the cytosolic domain of *Pb*UIS4. As a control for unspecific actin binding, cells were transfected with constructs expressing the cytosolic domain of *Pb*UIS3 (with a myc tag), another liver stage PVM protein, previously shown to interact with host autophagy marker microtubule-associated protein 1 light chain 3 (LC3) (Real et al., 2017). Western Blot analysis of co-immunoprecipitated proteins showed that the cytosolic domain of *Pb*UIS4, but not the cytosolic domain of *Pb*UIS3, interacts with actin (Figures 1F and S2B). This demonstrates that *Pb*UIS4 interacts with host cell actin via the former's cytosolic domain without requiring additional parasite proteins. However, the possibility that other host cell proteins may act as intermediaries or interacting partners cannot be excluded.
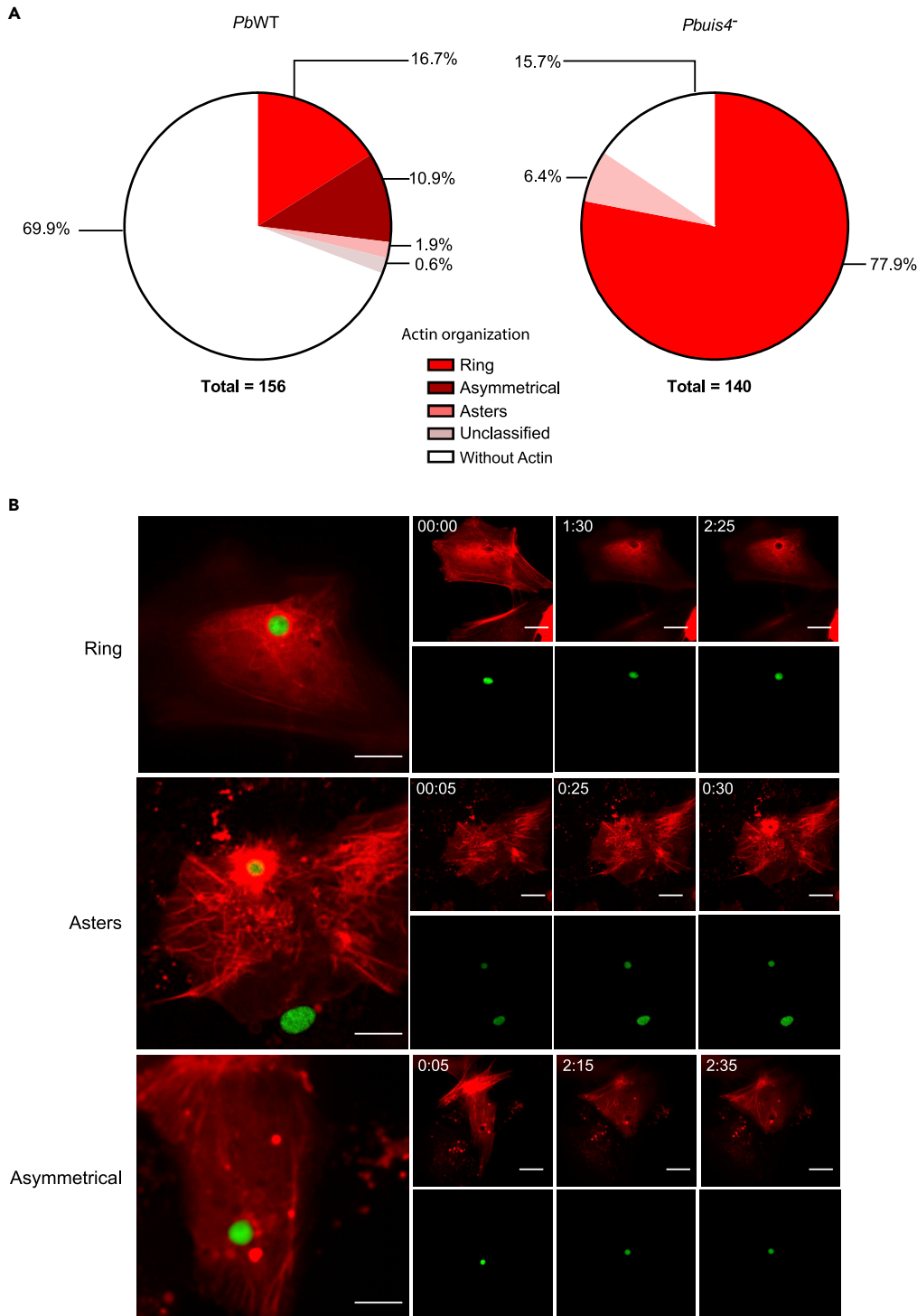
A

*Pb*WT

16.7%

10.9%

1.9%
0.6%

69.9%

Total = 156

Pbuis4⁻

15.7%

6.4%

77.9%

Total = 140

Actin organization
- ◼ Ring
- ◼ Asymmetrical
- ◼ Asters
- ◼ Unclassified
- ☐ Without Actin

B

Ring

Asters

Asymmetrical

00:00   1:30   2:25

00:05   0:25   0:30

0:05   2:15   2:35

Figure 2. Lack of UIS4 impacts host cell actin reorganization around the parasit

Huh7 cells were transfected with mCherry-LifeAct-expressing construct to label actin and infected 24 h later with *Pb*WT or *Pbuis4⁻* GFP-expressing parasites. Cells were imaged at 24 h.p.i., on a spinning disk confocal microscope (Zeiss Axio Observer, 63x Plan-Apochromat DIC-oil, Yokogawa CSU-x1), at an interval of 5 min per frame for a minimum of 6 h. Videos were analyzed with Imaris software (version 9.5). Videos with the cell or the parasite drifting out of frame, loss of mCherry expression or host cell death were excluded from analysis.

Figure 2. *Continued*

(A) Pie-chart indicating the distribution of actin structures (no structures-white, positive structures-pink to maroon) around the *Pb*WT and *Pbuis4⁻* parasites. Actin reorganization in parasite vicinity was classified as ring, asters, and asymmetrical. Some actin reorganization events remained unclassified.

(B) Representative time-lapse images of actin (red) structures around the EEF (green): Ring (top), asters (middle), and asymmetrical (bottom). Scale bar: 10 μm. An n = 156 (*Pb*WT) and 140 (*Pbuis4⁻*) EEFs in 3 independents experiments (transfection, infection and imaging).

Actin forms dynamic filaments that polymerize and depolymerize within the cell (Gawlitta et al., 1981). Therefore, to determine whether alterations in actin filaments could be observed in the presence of *Pb*UIS4, 3T3 fibroblast cells were transfected with a construct expressing the cytosolic domain of *Pb*UIS4. Cells were fixed 48 h after transfection, and actin structures were imaged by fluorescence microscopy. Reduced actin signal intensity was observed in cells expressing the *Pb*UIS4 cytosolic domain, when compared to neighboring non-transfected cells (Figures 1G and 1H; $p < 0.0001$). In contrast, cells transfected with the plasmid expressing the cytosolic domain of *Pb*UIS3 (used as a control) showed actin signal intensity similar to its non-transfected counterparts (Figures 1G and 1H; $p > 0.05$). Furthermore, the size of *Pbuis4*-transfected cells was significantly altered. A 51.7% reduction in cell size was observed in cells transfected with *Pbuis4* (and not *Pbuis3*), possibly as a result of the influence of *Pb*UIS4 on actin polymerization (Figures 1G and 1I; $p < 0.0001$). This was in agreement with a previously described correlation between cell size and filamentous actin in adipocytes (Hansson et al., 2019).

Increased dynamics of host actin structures around EEFs lacking UIS4

Having previously described actin reorganization events around the *Plasmodium* EEF in infected hepatocytes (Gomes-Santos et al., 2012), we proceeded to explore the significance of *Pb*UIS4-actin interaction during infection by following host actin dynamics around the EEF through long-term live microscopy. To that end, Huh7 cells expressing mCherry-LifeAct were infected with either *Pb*WT or *Pbuis4⁻* parasites (expressing GFP in cytosol) to visualize host filamentous actin real-time through infection. Time-lapse imaging was started at 24 h.p.i. with 5 min acquisition intervals on a spinning disk confocal microscope, to follow the host cell actin dynamics as the parasites developed.

We imaged 162 *Pb*WT and 143 *Pbuis4⁻* parasites. Nine videos in total (6 *Pb*WT and 3 *Pbuis4⁻* parasites) were excluded due to the infected cell or the parasite drifting out of the field of view during the acquisition. Actin polymerization events analyzed in these videos demonstrated that 30.13% of *Pb*WT parasites presented with frequent actin reorganization at the host-parasite interface, in contrast, these events were observed in 84.28% of *Pbuis4⁻* parasites (Figure 2A). The absence of UIS4, hence, led to a dramatic increase in the number of actin-based events around the developing parasites.

A plethora of patterns were observed in the reorganization of actin structures around both *Pb*WT and *Pbuis4⁻* parasites (Figure 2B). Ring-like actin structures were the most frequent, accounting for 16.67% and 77.86% of the observed events in *Pb*WT and *Pbuis4⁻* parasites, respectively (Figure 2A). The temporal dynamics of these structures around the parasite were also distinct. The formation of ring-like actin structures started with the asymmetric accumulation of actin in the EEF vicinity, which within 10 h, on average, generated a ring that surrounded the entire parasite (Figure 2B top panel). On the other hand, the formation of actin asters (a burst of actin that completely surrounds the parasite) was a much faster process, in which rings quickly expanded into asters and lasted for 45 min on average (Figure 2B middle panel). Actin asters were more prevalent in *Pbuis4⁻* (6.43%) than in *Pb*WT parasites (1.92%). In addition to the two aforementioned structures, we could also observe events of asymmetric actin accumulation that never completely encircled the parasite (asymmetrical actin bursts) (Figure 2B bottom panel). Asymmetric accumulation events occurred exclusively in *Pb*WT parasites (in 10.90% of the videos). These data clearly show that host cell actin dynamics is elevated in the absence of UIS4, at the EEF.

Actin activity around EEFs lacking UIS4 is associated with parasite elimination

P. berghei parasites lacking UIS4 have been previously shown to display impaired exoerythrocytic development with a reduction in the number of infected cells from 24 h.p.i. onwards (Mueller et al., 2005). We confirmed this observation in the UIS4-deficient *P. berghei* ANKA mutants (Figures 1A–1C and S1A–S1G) developed in-house. However, the mechanism driving *Pbuis4⁻* parasite clearance in hepatocytes remains to be elucidated. The higher frequency of actin reorganization observed around the
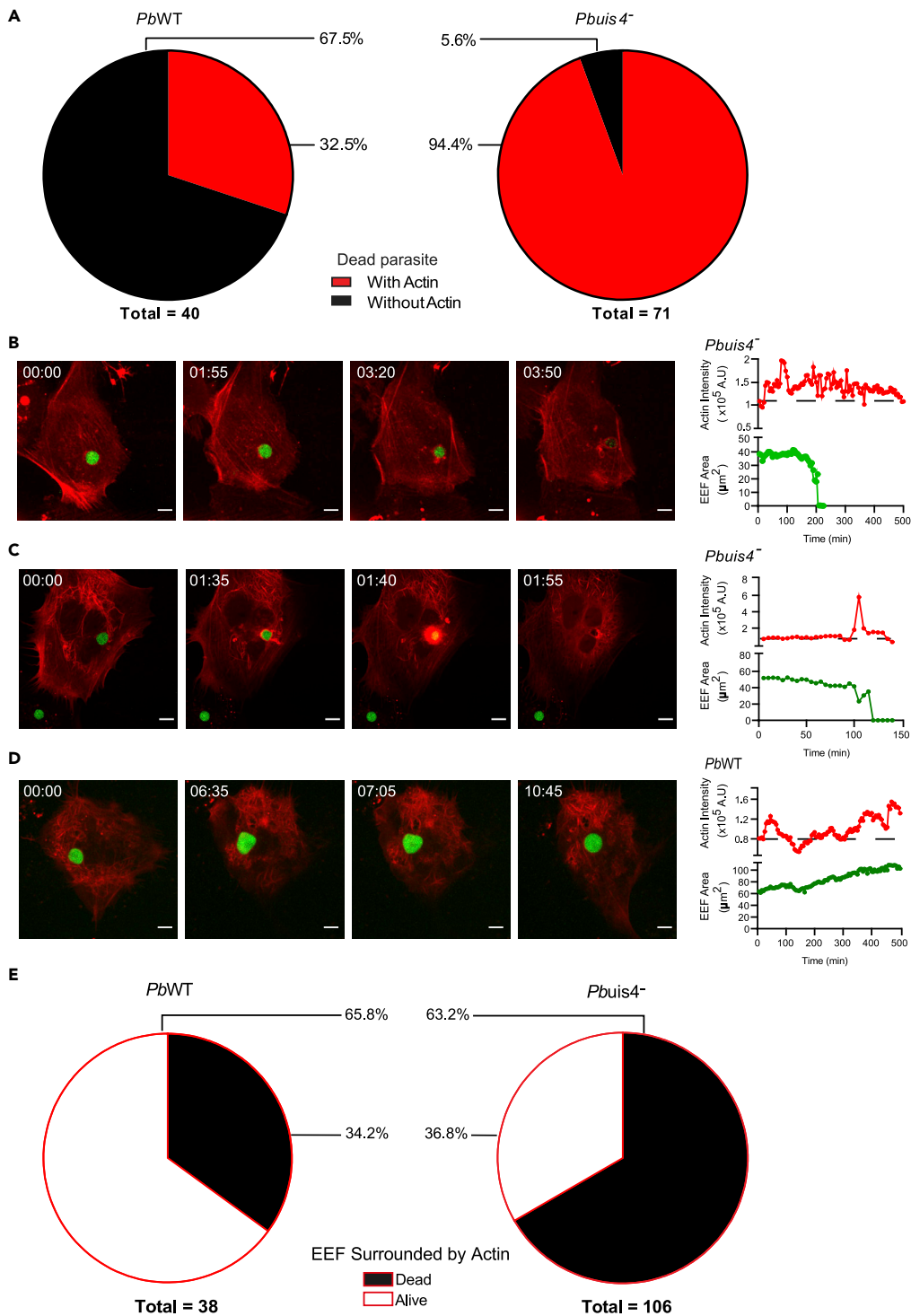
Figure 3. Increase in host cell actin dynamics is associated with parasite elimination

Huh7 cells were transfected with mCherry-LifeAct-expressing construct to label actin. Cells were infected with *Pb*WT or *Pbuis4⁻* GFP-expressing parasites, 24 h after transfection. Cells were imaged on a spinning disk confocal microscope 24 h.p.i. onwards, (Zeiss Axio Observer, 63x Plan-Apochromat DIC-oil, Yokogawa CSU-x1), at an interval of 5 min per frame for a minimum of 6 h. Time-lapse videos were analyzed with Imaris software (version 9.5). Videos with the cell or the parasite drifting out of frame, loss of mCherry expression or host cell death were excluded from analysis (A) Percentage of *Pb*WT (left) or *Pbuis4⁻* (right) parasites, eliminated either in association (red) or not (black) with local actin reorganization events as analyzed by live imaging.

Figure 3. Continued

(B, C, and D) representative micrographs of host actin (red) dynamics around parasites (green) through time, with respective plots showing actin signal intensity (red) and parasite area (green) in the Y axis relative to time (X axis).

(B) Ring-like actin organization around a *Pbuis4*⁻ EEF; (C) Aster-like actin organization around a *Pbuis4*⁻ EEF; and (D) Asymmetrical actin accumulation around a *Pb*WT EEF.

(E) Percentage of live (white) or dead (black) *Pb*WT and *Pbuis4*⁻ parasites in the presence of host actin association at 40 h.p.i.

(A) n = 40 (*Pb*WT) and 71 (*Pbuis4*⁻) EEFs in 3 independents experiments (transfection, infection, and imaging).

(E) n = 38 (*Pb*WT) and 106 (*Pbuis4*⁻) EEFs in 3 independents experiments (transfection, infection, and imaging). These videos are a subset of those reported in Figure 2, the 'n' represents the videos used for analysis, not the total videos imaged for this experiment. See also Figure S3 and Videos S1–S5.

Pbuis4⁻ parasites (with respect to *Pb*WT) led us to hypothesize that this phenomenon could be implicated in the significant reduction of *Pbuis4*⁻-infected hepatocytes. To test this hypothesis, we quantified the reorganization of actin structures in the vicinity of the EEFs that were eliminated during the acquisition period. We observed that 74 *Pb*WT parasites and 86 *Pbuis4*⁻ parasites were eliminated during image acquisition. Considering the parasites eliminated in live host cells only, we observed 44 (59.46%) of the *Pb*WT parasites and 77 (89.53%) of the *Pbuis4*⁻ parasites being eliminated. This strongly implies that UIS4 participates in a parasite mechanism of protection (Figure S3A). In the remaining videos (30 for *Pb*WT and 9 for *Pbuis4*⁻), the host cell died along with the parasite and was excluded from analysis. We further excluded from subsequent analysis cells that lost mCherry-LifeAct expression prior to parasite elimination as it precluded association of events to actin reorganization. Notably, 34.19% of the *Pb*WT and 57.72% of the *Pbuis4*⁻-analyzed EEFs were eliminated during the observation period (Figure S3B) of these association of death with actin structures occurred only in 32.50% of the *Pb*WT parasites; whereas 94.37% of the *Pbuis4*⁻ parasites that died were associated with actin polymerization events (Figure 3A), suggesting a link between an actin-dependent host cell defense mechanism and the lack of *Pb*UIS4.

The most common actin-associated process leading to *Pbuis4*⁻ disappearance was ring-like actin-driven events (89.55%), with the progressive decrease of parasite size, a process that could last for over 10 h. The images indicated a compression of EEF (Figure 3B and Video S1). Actin aster events were also associated with parasite elimination (10.45% of events) through a process that was faster than ring-like actin events, lasting frequently less than 1 h (Figure 3C and Video S2). We also report rare events of parasite fragmentation and subsequent extrusion (Figure S2C and Video S3), and ejection of an entire EEF without prior fragmentation (Figure S2D and Video S4).

The data also showed that *Pb*WT EEFs are more likely to evade host cell actin response than *Pbuis4*⁻ EEFs (an example is shown in Figure 3D and Video S5). 66% of *Pb*WT parasites associated with actin survived, while the survival rate of *Pbuis4*⁻ parasites was 36.79% (Figure 3E). Gomes-Santos et al. had previously described the involvement of the actin interacting protein-gelsolin in the prevalence of flashing actin rings around EEFs and subsequent clearance of parasites (Gomes-Santos et al., 2012). Following up on that line, we visualized the signal of gelsolin around *Pb*WT and *Pbuis4*⁻ EEFs at 24 h.p.i to understand whether a similar machinery is in action here as well. To that end, not only do we confirm the presence of gelsolin around EEFs but we also note that *Pbuis4*⁻ EEFs present with a lower signal relative to *Pb*WT (Figures S3F and S3G). Altogether, these observations indicate that *Pb*UIS4 can act in defense of the parasite and is employed to counter the cytoskeletal attacks of the host cell.

Parasite elimination depends on actomyosin complexes formed at the host-parasite interface

Our data so far suggest that the disappearance of the vast majority of the *Pbuis4*⁻ parasites occurs in association with an actin ring. Given that actin and myosin generate ring-like structures that contract in several biological processes such as cytokinesis and wound healing (Schwayer et al., 2016), we hypothesized that a similar mechanism could be responsible for the observed compression and parasite elimination. To test this hypothesis, host myosin-II was chemically inhibited with blebbistatin (Straight et al., 2003). Prolonged myosin-II inhibition leads to host cell cytotoxicity (Képiró et al., 2014; Mikulich et al., 2012). However, cells recover from short-term treatment within 4 h after removal of the compound (Figure S4). Thus, treatment with blebbistatin was carried out for 6 h only, starting at 24 h.p.i, as most EEF deaths were found to occur post 30 h.p.i (Figure S3E). Huh7 cells were infected with either *Pb*WT or *Pbuis4*⁻, and treated with 50 µM blebbistatin at 24 h.p.i, for 6 h. At 30 h.p.i, the compound was washed with PBS and cells were incubated in drug-free medium until 48 h.p.i. Cells were then fixed and parasite numbers and size were assessed by
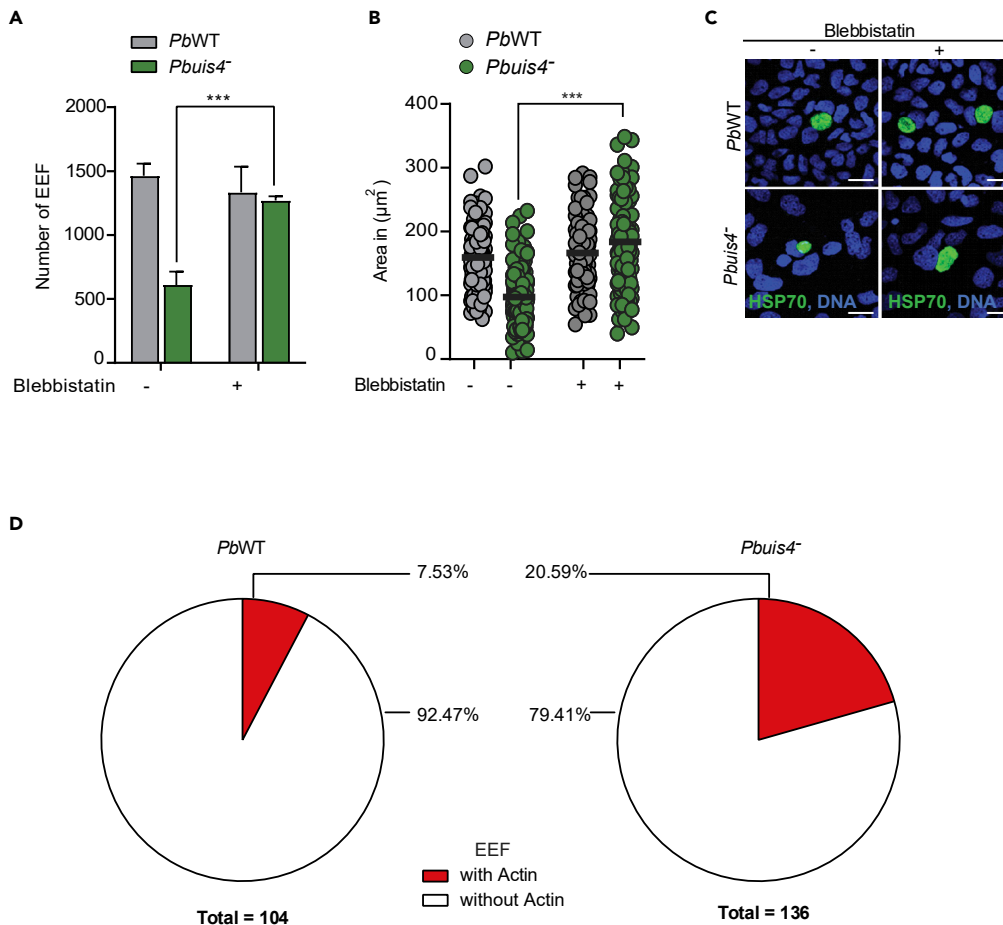
Figure 4. Parasite elimination is mediated by host actomyosin complexes

(A, B, and C) Huh7 cells were infected with either *Pb*WT (gray bars or symbols) or *Pb*uis4- (green bars or symbols) parasites, treated with 50 μM blebbistatin for 6 h, fixed at 48 h.p.i., and immunostained with anti-*Pb*HSP70 and Hoechst (n = 3). A number of exoerythrocytic forms (EEFs), (B) EEF size as measured by the area (each symbol represents one EEF) and, (C) Representative micrographs of quantified EEFs (HSP70-green, DNA-blue, scale bar: 10 μm) for control (−) or blebbistatin (+) treated cells infected cells.

(D) Huh7 cells were transfected with mCherry-LifeAct-expressing construct to label actin and infected with *Pb*WT or *Pb*uis4-parasites (GFP-expressing motherline). Cells were treated with 50 μM blebbistatin at 24 h.p.i. for a period of 6 h, followed by drug washout. Samples were imaged on a spinning disk confocal microscope (Zeiss Axio Observer, 63x Plan-Apochromat DIC-oil, Yokogawa CSU-x1), at an interval of 10 min per frame for 7 to 8 h. Videos were analyzed with Imaris software (version 9.5). Videos with the cell or the parasite drifting out of frame, loss of mCherry expression, or host cell death were excluded from analysis. Pie-charts showing the percentage of *Pb*WT (left) and *Pb*uis4- (right) parasites with (red) or without (white) local host cell actin reorganization events after blebbistatin treatment. Data in A are represented as mean ± SEM, data in (B) are represented as individual data points, with line representing the mean. Statistical analysis of was performed using two-tailed Mann-Whitney U test, ns represents $p > 0.05$; and ***$p < 0.005$.

(A) n = 4293 (*Pb*WT, untreated), 1818 (*Pb*uis4-, untreated), 3917 (*Pb*WT, blebbistatin-treated), and 3790 (*Pb*uis4-, blebbistatin-treated) and (B) n ∼ 900 (*Pb*WT and *Pb*uis4-) EEFs in 3 independent experiments. (D) n = 104 (*Pb*WT) and 136 (*Pb*uis4-) EEFs with blebbistatin treatment in 3 independent experiments. See also Figure S4.

immunofluorescence microscopy. No difference in the number of EEF was observed between the treated and the untreated *Pb*WT parasites (Figure 4A, p = 0.6), suggesting that *Pb*WT parasites are capable of preventing or escaping the force generated by host myosin-II. Interestingly, inhibition of host myosin-II was sufficient to rescue the survival (p < 0.001) and development (p < 0.001) of the *Pb*uis4- parasites (Figures 4A–4C). To determine whether this was due to the lack of ring-like actin structures in the EEF vicinity, infected Huh7 cells were monitored after myosin-II inhibition by live imaging, as described previously. mCherry-LifeAct-expressing Huh7 cells were infected and treated with blebbistatin 24 h.p.i for a

period of 6 h. At the end of the treatment, the compound was washed out and replaced with phenol red-free DMEM for imaging. The frequency of actin structures in the EEF vicinity upon blebbistatin treatment was 7.53% and 20.59% in *Pb*WT and *Pbuis4⁻* parasites, respectively (Figure 4D) which was diminished from the 30.12% and 84.29% previously observed without treatment (Figure 2A). There, hence, is some form of engagement between the host actomyosin machinery and *Pb*UIS4, which seems to determine the survival of the EEF. Taken together, these data show that the PVM protein *Pb*UIS4 interacts with host cell actin, affecting its polymerization and possibly protecting the parasite from the compression generated by host actomyosin complexes at the host-parasite interface. It shows that *Pb*UIS4 is an essential *Plasmodium* protein required for parasite evasion from the host-cell autonomous defenses.

DISCUSSION

Pathogens that adopt an intracellular lifestyle, whether prokaryotes or eukaryotes, often escape challenges such as complement or neutralizing-antibodies, which threaten their extracellular counterparts. However, upon entering the host cell, they encounter a barrage of host-cell autonomous defense mechanisms, such as autophagy, which limit their development. Possibly, because of that pressure, many intracellular micro-organisms have evolved to live inside a vacuolar compartment within the host cell. In the case of *Plasmodium*, the membrane delimiting this compartment—the PVM—is decorated by proteins critical for the maintenance of the infection (Mueller et al., 2005; Orito et al., 2013; Real et al., 2017). We have previously shown that the continuous replenishment of the PVM-resident proteins is necessary for parasite viability (Hanson et al., 2013; Itoe et al., 2014). However, the functional role of these proteins is only now starting to be unveiled. We have recently shown that *Plasmodium* UIS3 sequesters host LC3 to avoid elimination by autophagy in hepatocytes (Real et al., 2017) and that disruption of that interaction by a small molecule causes parasite elimination from host cells (Setua et al., 2020). We now show that *Plasmodium* parasites have devised a different way to avoid elimination by a distinct host-cell-intrinsic mechanism. Our data clearly show that the ability of the PVM-resident protein- *Pb*UIS4 to interact with host cell actin and alter the latter's organization and dynamics around the growing parasite, thereby protecting the former from actin-dependent elimination. Indeed, while *Pb*WT parasites present few events of actin reorganization in their vicinity, the *Pbuis4⁻* parasites (besides showing a reduction of lysosomes surrounding the PVM (Petersen et al., 2017), which may or may not be connected to a host autophagy response) are surrounded by dense rings of actin, which precede parasite disappearance and elimination. These dynamics are a part of coordinated events facilitated by host actomyosin complexes, through which compressive forces are generated around the parasite in the absence of the UIS4 protein. Disruption of the host actomyosin machinery rescued the survival of *Pbuis4⁻* parasites, without enhancing the survival of *Pb*WT parasites, leading us to speculate the UIS4 may interfere with the recruitment/assembly of actin-interacting partners thereby inhibiting the formation of active actin structures around the WT EEF. Interestingly, the formation of active actin structures was shown to depend on the local concentration of its interacting proteins such as myosin-II, and the latter itself is also capable to self-organize the former into rings (Backouche et al., 2006).

The role of host actin during intracellular infections has been extensively described for bacteria wherein actin may be manipulated to favor pathogen entry, exit, stabilization of pathogenic vacuole, or for diversion of host vesicles among other roles (Colonne et al., 2016). As for *Plasmodium*, studies during blood stages have indicated substantial manipulation of host cell actin (Cyrklaff et al., 2011; Deitsch and Wellems, 1996; Millholland et al., 2011; Oh et al., 2000; Pei et al., 2007), while little is known in regards to the liver stages. Previous observations from our lab identified the curious nature of actin flashing around young EEFs which was associated with parasite clearance and, described the involvement of gelsolin in formation of such actin rings (Gomes-Santos et al., 2012). However, we observe a decline in the gelsolin signal around *Pbuis4⁻* EEFs at time points shortly preceding those where we observe reduction in EEF numbers relative to *Pb*WT. Gelsolin is an actin-interacting protein, which functions in severing F-actin, and therefore reducing the efficiency of actomyosin bridge formation (Sakamoto et al., 2020). Enhanced occurrence of actin rings around the *Pbuis4⁻* EEFs put together with a reduction in gelsolin levels there can help explain one possible way wherein the parasite is unable to escape such actomyosin structures. While we do not detect gelsolin as a direct interactor of *Pb*UIS4 in the IP, there is a possibility that it may be recruited there via actin or other host proteins associating with actin around the EEF, as gelsolin was shown participating in actomyosin activity (Vemula et al., 2021). It is interesting though that Gomes-Santos et al., while observing reduction in actin rings around the EEFs upon knocking down gelsolin, do not report any dramatic alteration in parasite survival in this case (Gomes-Santos et al., 2012). One may speculate that gelsolin may be exploited by *Pb*WT parasites to avoid continuous actin network formation

around the PV, and removal of gelsolin would not affect parasite survival, while *Pbuis4⁻* is lacking in such capacities to escape the host actomyosin insult.

Nevertheless, the possible role of actomyosin in generating contractile forces around the EEF paired with reduced gelsolin levels around parasites which known to be cleared by such actin ring-like structures creates for an exciting area for investigation regarding the machinery employed by the host as a cytosolic defense against an intracellular pathogen. The present study helps in addressing the gap in knowledge regarding parasite components involved in eluding this actin-mediated clearance. In addition, to following up on the previous work, we identify for the first time to the best of our knowledge a role of the PVM resident (*Pb*UIS4) in the regulation of host actin dynamics around the EEF, which in turn may serve to ensure parasite survival in hepatocytes.

The fine-tuning of the host actin machinery, as key to a successful liver stage *Plasmodium* infection, creates opportunities to investigate novel mechanisms of host modulation and the role of the host actin interactome as a cell-mediated defense system during such infections. This would be particularly interesting for the case of *Plasmodium vivax* EEFs, which show differential distribution of *Pv*UIS4 between growing schizonts and hypnozoites. Recombinant monoclonal antibody against *Pv*UIS4 stains both the replicating liver stages and the dormant hypnozoites, but allows for a reliable discrimination between the two forms due to the hypnozoite-specific UIS4-positive PVM prominence (Schafer et al., 2018). How hypnozoites manage to escape host actin-based defenses despite their smaller size and whether *Pv*UIS4 is involved in this process remain an exciting area to explore. This may also help to elucidate mechanisms of hypnozoite survival, opening avenues to disrupt the same as an anti-plasmodial intervention strategy.

Limitations of the study

One main question remains open from this study. What is the mechanism by which UIS4 controls actin activity around the EEF, and in vicinity of the PVM? It is tempting to hypothesize a potential role of UIS4 in interfering with host actin polymerization. While several attempts were made in order to test this hypothesis, the inconclusive results do not allow us to claim UIS4 as an active agent in depolymerization of host actin on its own. In fact, they lead us to suspect that, although from the parasite side UIS4 was sufficient for an effect on host cell actin, other host players must be required for this effect to be observed. In the future, different actin-associated proteins from the host side can be screened to dissect the machinery responsible for this actin activity around the parasite. This approach has the potential to highlight novel candidates mediating host-cell autonomous defenses during infection to ensure parasite survival in hepatocytes.

STAR★METHODS

Detailed methods are provided in the online version of this paper and include the following:

- KEY RESOURCES TABLE
- RESOURCE AVAILABILITY
  - Lead contact
  - Materials availability
  - Data and code availability
- EXPERIMENTAL MODEL AND SUBJECT DETAILS
  - Animal work
  - *Pbuis4⁻* parasite generation
  - Genotype and phenotype validation of the transgenic parasites
  - Sporozoites purification
  - Mice infection
  - Hepatoma cell line infection
- METHOD DETAILS
  - cDNA synthesis and real-Time PCR
  - Cell transfection
  - Immunoprecipitation
  - Western blot
  - Silver staining
  - Mass spectrometry analysis

- ○ Blebbistatin treatment
- ○ Immunofluorescence assay
- ○ Live imaging experiments and image analysis
- ● QUANTIFICATION AND STATISTICAL ANALYSIS

AUTHOR CONTRIBUTIONS

Conceptualization: M.M.M; Investigation: V.M'B., A.L.; Writing – Original draft: V.M'B., M.M.M.; Writing – Review and Editing: V.M'B., A.L., S.M., K.S., M.M.M.; Supervision: K.S., M.M.M.; Funding Acquisition: M.M.M.

DECLARATION OF INTERESTS

Authors declare no competing interests.

REFERENCES

Backouche, F., Haviv, L., Groswasser, D., and Bernheim-Groswasser, A. (2006). Active gels: dynamics of patterning and self-organization. Phys. Biol. 3, 264–273. https://doi.org/10.1088/1478-3975/3/4/004.

Colonne, P.M., Winchell, C.G., and Voth, D.E. (2016). Hijacking host cell highways: manipulation of the host actin cytoskeleton by obligate intracellular bacterial pathogens. Front. Cell. Infect. Microbiol. 6, 107. https://doi.org/10.3389/fcimb.2016.00107.

Cyrklaff, M., Sanchez, C.P., Kilian, N., Bisseye, C., Simpore, J., Frischknecht, F., and Lanzer, M. (2011). Hemoglobins S and C interfere with actin remodeling in Plasmodium falciparum-infected erythrocytes. Science 334, 1283–1286. https://doi.org/10.1126/science.1213775.

Deitsch, K.W., and Wellems, T.E. (1996). Membrane modifications in erythrocytes parasitized by Plasmodium falciparum. Mol. Biochem. Parasitol. 76, 1–10. https://doi.org/10.1016/0166-6851(95)02575-8.

Gawlitta, W., Stockem, W., and Weber, K. (1981). Visualization of actin polymerization and depolymerization cycles during polyamine-induced cytokinesis in living Amoeba proteus. Cell Tissue Res. 215, 249–261. https://doi.org/10.1007/bf00239112.

Gomes-Santos, C.S.S., Itoe, M.A., Afonso, C., Henriques, R., Gardner, R., Sepúlveda, N., Simões, P.D., Raquel, H., Almeida, A.P., Moita, L.F., et al. (2012). Highly dynamic host actin reorganization around developing Plasmodium inside hepatocytes. PLoS One 7, e29408. https://doi.org/10.1371/journal.pone.0029408.

Hanson, K.K., Ressurreição, A.S., Buchholz, K., Prudêncio, M., Herman-Ornelas, J.D., Rebelo, M., Beatty, W.L., Wirth, D.F., Hänscheid, T., Moreira, R., et al. (2013). Torins are potent antimalarials that block replenishment of Plasmodium liver stage parasitophorous vacuole membrane proteins. Proc. Natl. Acad. Sci. U S A 110, E2838–E2847. https://doi.org/10.1073/pnas.1306097110.

Hansson, B., Morén, B., Fryklund, C., Vliex, L., Wasserstrom, S., Albinsson, S., Berger, K., and Stenkula, K.G. (2019). Adipose cell size changes are associated with a drastic actin remodeling. Sci. Rep. 9, 12941. https://doi.org/10.1038/s41598-019-49418-0.

Itoe, M.A., Sampaio, J.L., Cabal, G.G., Real, E., Zuzarte-Luis, V., March, S., Bhatia, S.N., Frischknecht, F., Thiele, C., Shevchenko, A., and Mota, M. (2014). Host cell phosphatidylcholine is a key mediator of malaria parasite survival during liver stage infection. Cell Host Microbe 16, 778–786. https://doi.org/10.1016/j.chom.2014.11.006.

Janse, C.J., Franke-Fayard, B., Mair, G.R., Ramesar, J., Thiel, C., Engelmann, S., Matuschewski, K., van Gemert, G.J., Sauerwein, R.W., and Waters, A.P. (2006a). High efficiency transfection of Plasmodium berghei facilitates novel selection procedures. Mol. Biochem. Parasitol. 145, 60–70. https://doi.org/10.1016/j.molbiopara.2005.09.007.

Janse, C.J., Ramesar, J., and Waters, A.P. (2006b). High-efficiency transfection and drug selection of genetically transformed blood stages of the rodent malaria parasite Plasmodium berghei. Nat. Protoc. 1, 346–356. https://doi.org/10.1038/nprot.2006.53.

Kaiser, K., Matuschewski, K., Camargo, N., Ross, J., and Kappe, S.H.I. (2004). Differential transcriptome profiling identifies Plasmodium genes encoding pre-erythrocytic stage-specific

proteins. Mol. Microbiol. *51*, 1221–1232. https://doi.org/10.1046/j.1365-2958.2003.03909.x.

Képiró, M., Várkuti, B.H., Végner, L., Vörös, G., Hegyi, G., Varga, M., and Málnási-Csizmadia, A. (2014). Para-nitroblebbistatin, the non-cytotoxic and photostable myosin II inhibitor. Angew. Chem. Int. Ed. *53*, 8211–8215. https://doi.org/10.1002/anie.201403540.

Liehl, P., Zuzarte-Luis, V., and Mota, M.M. (2015). Unveiling the pathogen behind the vacuole. Nat. Rev. Microbiol. *13*, 589–598. https://doi.org/10.1038/nrmicro3504.

Madeira, F., Park, Y.M., Lee, J., Buso, N., Gur, T., Madhusoodanan, N., Basutkar, P., Tivey, A.R.N., Potter, S.C., Finn, R.D., and Lopez, R. (2019). The EMBL-EBI search and sequence analysis tools APIs in 2019. Nucleic Acids Res. *47*, W636–W641. https://doi.org/10.1093/nar/gkz268.

Meireles, P., Mendes, A.M., Aroeira, R.I., Mounce, B.C., Vignuzzi, M., Staines, H.M., and Prudêncio, M. (2017). Uptake and metabolism of arginine impact Plasmodium development in the liver. Sci. Rep. *7*, 4072. https://doi.org/10.1038/s41598-017-04424-y.

Mikulich, A., Kavaliauskiene, S., and Juzenas, P. (2012). Blebbistatin, a myosin inhibitor, is phototoxic to human cancer cells under exposure to blue light. Biochim. Biophys. Acta Gen. Subj. *1820*, 870–877. https://doi.org/10.1016/j.bbagen.2012.04.003.

Millholland, M.G., Chandramohanadas, R., Pizzarro, A., Wehr, A., Shi, H., Darling, C., Lim, C.T., and Greenbaum, D.C. (2011). The malaria parasite progressively dismantles the host erythrocyte cytoskeleton for efficient egress. Mol. Cell. Proteomics *10*. M111.010678. https://doi.org/10.1074/mcp.m111.010678.

Mueller, A.-K., Camargo, N., Kaiser, K., Andorfer, C., Frevert, U., Matuschewski, K., and Kappe, S.H.I. (2005). Plasmodium liver stage developmental arrest by depletion of a protein at the parasite-host interface. Proc. Natl. Acad. Sci. U S A *102*, 3022–3027. https://doi.org/10.1073/pnas.0408442102.

Oh, S.S., Voigt, S., Fisher, D., Yi, S.J., LeRoy, P.J., Derick, L.H., Liu, S.C., and Chishti, A.H. (2000). Plasmodium falciparum erythrocyte membrane protein 1 is anchored to the actin-spectrin junction and knob-associated histidine-rich protein in the erythrocyte skeleton. Mol. Biochem. Parasitol. *108*, 237–247. https://doi.org/10.1016/s0166-6851(00)00227-9.

Orito, Y., Ishino, T., Iwanaga, S., Kaneko, I., Kato, T., Menard, R., Chinzei, Y., and Yuda, M. (2013). Liver-specific protein 2: a Plasmodium protein exported to the hepatocyte cytoplasm and

required for merozoite formation. Mol. Microbiol. *87*, 66–79. https://doi.org/10.1111/mmi.12083.

Pei, X., Guo, X., Coppel, R., Mohandas, N., and An, X. (2007). Plasmodium falciparum erythrocyte membrane protein 3 (PfEMP3) destabilizes erythrocyte membrane skeleton. J. Biol. Chem. *282*, 26754–26758. https://doi.org/10.1074/jbc.m701612200.

Petersen, W., Stenzel, W., Silvie, O., Blanz, J., Saftig, P., Matuschewski, K., and Ingmundson, A. (2017). Sequestration of cholesterol within the host late endocytic pathway restricts liver-stage *Plasmodium* development. Mol. Biol. Cell *28*, 726–735. https://doi.org/10.1091/mbc.e16-07-0531.

Prudêncio, M., Rodriguez, A., and Mota, M.M. (2006). The silent path to thousands of merozoites: the Plasmodium liver stage. Nat. Rev. Microbiol. *4*, 849–856. https://doi.org/10.1038/nrmicro1529.

Real, E., Rodrigues, L., Cabal, G.G., Enguita, F.J., Mancio-Silva, L., Mello-Vieira, J., Beatty, W., Vera, I.M., Zuzarte-Luís, V., Figueira, T.N., et al. (2017). Plasmodium UIS3 sequesters host LC3 to avoid elimination by autophagy in hepatocytes. Nat. Microbiol. *3*, 17–25. https://doi.org/10.1038/s41564-017-0054-x.

Sá e Cunha, C., Nyboer, B., Heiss, K., Sanches-Vaz, M., Fontinha, D., Wiedtke, E., Grimm, D., Przyborski, J.M., Mota, M.M., Prudêncio, M., and Mueller, A.K. (2017). *Plasmodium berghei* EXP-1 interacts with host Apolipoprotein H during *Plasmodium* liver-stage development. Proc. Natl. Acad. Sci. U S A *114*, E1138–E1147. https://doi.org/10.1073/pnas.1606419114.

Sakamoto, R., Tanabe, M., Hiraiwa, T., Suzuki, K., Ishiwata, S., Maeda, Y.T., and Miyazaki, M. (2020). Tug-of-war between actomyosin-driven antagonistic forces determines the positioning symmetry in cell-sized confinement. Nat. Commun. *11*, 3063. https://doi.org/10.1038/s41467-020-16677-9.

Schafer, C., Dambrauskas, N., Steel, R.W., Carbonetti, S., Chuenchob, V., Flannery, E.L., Vigdorovich, V., Oliver, B.G., Roobsoong, W., Maher, S.P., et al. (2018). A recombinant antibody against Plasmodium vivax UIS4 for distinguishing replicating from dormant liver stages 11 Medical and Health Sciences 1108 Medical Microbiology. Malar. J. *17*, 1–10.

Schindelin, J., Arganda-Carreras, I., Frise, E., Kaynig, V., Longair, M., Pietzsch, T., Preibisch, S., Rueden, C., Saalfeld, S., Schmid, B., et al. (2012). Fiji: an open-source platform for biological-image analysis. Nat. Methods *9*, 676–682. https://doi.org/10.1038/nmeth.2019.

Schwayer, C., Sikora, M., Slováková, J., Kardos, R., and Heisenberg, C.P. (2016). Actin rings of power. Dev. Cell *37*, 493–506. https://doi.org/10.1016/j.devcel.2016.05.024.

Setua, S., Enguita, F.J., Chora, Â.F., Rangaprasad, H., Lahree, A., Marques, S., Sundaramurthy, V., and Mota, M.M. (2020). Disrupting Plasmodium UIS3–host LC3 interaction with a small molecule causes parasite elimination from host cells. Commun. Biol. *3*, 688. https://doi.org/10.1038/s42003-020-01422-1.

Slavic, K., Krishna, S., Lahree, A., Bouyer, G., Hanson, K.K., Vera, I., Pittman, J.K., Staines, H.M., and Mota, M.M. (2016). A vacuolar iron-transporter homologue acts as a detoxifier in Plasmodium. Nat. Commun. *7*, 10403. https://doi.org/10.1038/ncomms10403.

Slavic, K., Straschil, U., Reininger, L., Doerig, C., Morin, C., Tewari, R., and Krishna, S. (2010). Life cycle studies of the hexose transporter of Plasmodium species and genetic validation of their essentiality. Mol. Microbiol. *75*, 1402–1413. https://doi.org/10.1111/j.1365-2958.2010.07060.x.

Spielmann, T., Montagna, G.N., Hecht, L., and Matuschewski, K. (2012). Molecular make-up of the Plasmodium parasitophorous vacuolar membrane. Int. J. Med. Microbiol. *302*, 179–186. https://doi.org/10.1016/j.ijmm.2012.07.011.

Straight, A.F., Cheung, A., Limouze, J., Chen, I., Westwood, N.J., Sellers, J.R., and Mitchison, T.J. (2003). Dissecting temporal and spatial control of cytokinesis with a myosin II inhibitor. Science *299*, 1743–1747. https://doi.org/10.1126/science.1081412.

Thieleke-Matos, C., Lopes da Silva, M., Cabrita-Santos, L., Portal, M.D., Rodrigues, I.P., Zuzarte-Luis, V., Ramalho, J.S., Futter, C.E., Mota, M.M., Barral, D.C., and Seabra, M.C. (2016). Host cell autophagy contributes to Plasmodium liver development. Cell. Microbiol. *18*, 437–450. https://doi.org/10.1111/cmi.12524.

Tsuji, M., Mattei, D., Nussenzweig, R.S., Eichinger, D., and Zavala, F. (1994). Demonstration of heat-shock protein 70 in the sporozoite stage of malaria parasites. Parasitol. Res. *80*, 16–21. https://doi.org/10.1007/bf00932618.

Vemula, V., Huber, T., Ušaj, M., Bugyi, B., and Månsson, A. (2021). Myosin and gelsolin cooperate in actin filament severing and actomyosin motor activity. J. Biol. Chem. *296*, 100181. https://doi.org/10.1074/jbc.ra120.015863.

World Health Organization (2020). World Malaria Report: 20 Years of Global Progress and Challenges (World Health Organization).

STAR★METHODS

KEY RESOURCES TABLE

REAGENT or RESOURCE	SOURCE	IDENTIFIER
Antibodies		
Polyclonal antibody Goat anti-UIS4	SICGEN	Cat# AB0042-200; RRID: AB_2333158
Polyclonal antibody rabbit anti-actin	Sigma	Cat# A2066; RRID: AB_476693
Monoclonal antibody mouse anti c-myc tag	MBL lifesciences	Cat# M192-3; RRID: AB_11160947
Monoclonal antibody anti-HSP70 (2E6)	(Tsuji et al., 1994)	RRID: AB_2650482
Antibody Mouse anti-rabbit HRP	Nordic MUBio	Cat# X1207M
GFP-Polyclonal Antibody Alexa Fluor 488	Invitrogen	Cat# A-21311; RRID: AB_221477
Alexa Fluor® 488 anti-HA.11 Epitope Tag Antibody	Biolegend	Cat# 901509; RRID: AB_2565072
Alexa Fluor 647 goat anti-mouse igG,	Thermo Scientific	Cat# A21236; RRID: AB_2535805
Alexa Fluor® 568 donkey anti-goat IgG (H + L)	Thermo Scientific	Cat# A11057; RRID: AB_2534104
Hoechst 33342	Invitrogen	Cat# H1399
Bacterial and virus strains		
E. coli BL21(DE3)	Nzytech	Cat# MB006
Competent cell _ XL10-Gold Ultracompetent Cells	Agilent	Cat# 200315
Biological samples		
C57Bl/6J Mouse Liver	This study	NA
BALB/cJ Mouse Blood	This study	NA
Chemicals, peptides, and recombinant proteins		
(+)-Blebbistatin	Bio Vision	Cat# BV-2407-1
CytoPainter Phalloidin-iFluor 647 Reagent	Abcam	Cat# ab176759
Fugene 6 Transfection reagent	Promega	Cat# PROME2691
Paraformaldehyde 4% (PFA)	ChemCruz	Cat# sc-281692
Acetic Glacial Acid	SAFC	Cat#ARK2183
Proteases inhibitors: cOmplete(TM), EDTA-free Protease Inhibit	Roche	Cat# 11873580001
Triton X-100	Sigma	Cat# 9002-93-1
Amphotericin B (Fungizone)	Gibco	Cat#15290018
Gentamicin	Gibco	Cat#15750-037
Phenylmethanesulfonylfluoride (PMSF)	Sigma	Cat#P7626-250MG
Fluoromount-G	Thermo fisher	Cat# 00-4958-02
Nycodenz	Axis-Shield	Cat# 1002424
Albumin Bovine Fraction V (BSA)	Nzytech	Cat# MB04602
Saponin	Sigma	Cat# 47036
KpnI	New England Bioloabs	Cat# R0142S
ApaI	New England Bioloabs	Cat# R0114S
Phusion™ High-Fidelity DNA Polymerase (2 U/μL)	Thermo Scientific	Cat# F530S
T4 DNA Ligase	New England Bioloabs	Cat# M0202S
Critical commercial assays		
Silver Stain Kit- PROTSIL1-1KT	Sigma	Cat# PROTSIL2-1KT
Silver Stain kit	Thermo Scientific	Cat## 24612
Dynabeads Protein G	Invitrogen	Cat# 10004D
Protein quantification: Pierce™ BCA Protein Assay Kit	Thermo Scientific	Cat#23227

Continued

REAGENT or RESOURCE	SOURCE	IDENTIFIER
DNA extraction kit	Qiagen	Cat# 51604
RNA extraction kit	NZYTech	Cat# MB13402
PureZol RNA extraction reagent	Bio Rad	Cat# 7326890
CloneJET PCR Cloning Kit	Thermo Scientific	Cat# K1231
QIAquick Gel Extraction Kit	Qiagen	Cat# 28706X4
QIAquick PCR Purification Kit	Qiagen	Cat# 28104
iTaq Universal SYBR Green Supermix	Bio-Rad	Cat# 1725124
NZYTaq II 2x Green Master Mix	Nzytech	Cat# MB358
Deposited data		
MBana_Video S1	This study	Video S1_Re_Figure 3B
MBana_Video S2	This study	Video S2_Re_Figure 3C
MBana_Video S3	This study	Video S3_Re_Figure S2C
MBana_Video S4	This study	Video S4_Re_Figure S2D
MBana_Video S5	This study	Video S5_Re_Figure 3D
Mass Spectrometry Analysis of raw data with Mascot Search Results list	This study	Mendeley Data: https://doi.org/10.17632/3mxjfyc7d6.1
Experimental models: Cell lines		
Human hepatoma cell line_ Huh7	NIBIOHN, Japan	JCRB0403
Human Hepatoma cell line_HepG2 cell line	ATCC	Cat#HB-8065
Embryonic Kidney cell line HEK-293	ATCC	Cat# CRL-1573
3T3 cell line	ATCC	Cat#CRL-1658
Experimental models: Organisms/strains		
C57Bl/6J Mice	Charles River	NA
BALB/cJ Mice	Charles River	NA
GFP-expressing *Plasmodium berghei* ANKA-WT	(Janse et al., 2006a)	Leiden Malaria Research Group line-507cl1
*Plasmodium berghei uis*4⁻ (*Pbuis*4⁻)	This study	Pbuis4⁻(clone 3)
Anopheles *Stephensis* Mosquito	Instituto de Medicina Molecular, João Lobo Antunes	NA
Oligonucleotides		
*Pbuis*4 5′UTR forward – GGTACCTGGATTCATTTTTTGATGCATGC	This study	NA
*Pbuis*4 5′UTR reverse– GGGCCCTTTATTCAGACGTAATAATTATGTGC	This study	NA
*Pbuis*4 3′UTR forward – AAGATATCATAATTCATTATGAGTAGTGTAATTCAG	This study	NA
*Pbuis*4 3′UTR forward – AAGATATCATAATTCATTATGAGTAGTGTAATTCAG	This study	NA
*Pbuis*4 3′UTR reverse – GCGGCCGCAAGTTTGCATATACGGCTGCTTCC	This study	NA
*Pbuis*4 locus forward - TCTGCGATTTTTCTTATATTTACTATTAA	This study	NA
*Pbuis*4 locus reverse - TTTTTTACATATGTTGTATGCATAACATG	This study	NA
Tgdhfr forward - CAATGATTCATAAATAGTTGGACTTG	(Slavic et al., 2016)	NA
Tgdhfr reverse - GATGTGTTATGTGATTAATTCATACAC	(Slavic et al., 2016)	NA

(Continued on next page)

Continued

REAGENT or RESOURCE	SOURCE	IDENTIFIER
Pbuis4 forward - AAGGTACCCCACATACGTTTCTCT ATTTTTTATC	This study	NA
Pbuis4 reverse - TTGGGCCCTATGTATGGGCCGAATGATTT	This study	NA
*Pb*18S forward - AAGCATTAAATAAAGCGAATA CATCCTTAC	(Slavic et al., 2016)	NA
*Pb*18S reverse - GGAGATTGGTTTTGACGTTTATGTG	(Slavic et al., 2016)	NA
Mmhprt forward – TTTGCTGACCTGCTGGATTAC	(Meireles et al., 2017)	NA
Mmhprt reverse - CAAGACATTCTTTCCAGTTAAAGTTG	(Meireles et al., 2017)	NA
Hshprt forward – TTTGCTGACCTGCTGGATTAC	(Meireles et al., 2017)	NA
Hshprt reverse - CAAGACATTCTTTCCAGTTAAAGTTG	(Meireles et al., 2017)	NA
Recombinant DNA		
Pbvit knockout Plasmid	(Slavic et al., 2016)	pPbvit ko
Pbuis4⁻ generation Plasmid	This study	p*Pbuis4-*
pCMV-HA-PbUIS4	(Real et al., 2017)	pCMV-HA-PbUIS4
pCMV-MYC-sPbUIS3	(Real et al., 2017)	pCMV-MYC-sPbUIS3
mCherry-LifeAct plasmid	Addgene (gift from Michael Davidson)	Cat # 54491
Software and algorithms		
Imaris	Imaris RRID:SCR_007370	https://imaris.oxinst.com/
Fiji	(Schindelin et al., 2012)	https://www.nature.com/articles/ nmeth.2019?page=15
ZEN-Blue Edition	Zeiss	https://www.zeiss.com/microscopy/int/ products/microscope-software/zen.html
ZEN-Black Edition	Zeiss	https://www.zeiss.com/microscopy/int/ products/microscope-software/zen.html
Prism	GraphPad Prism version 8.4.3for Windows, GraphPad Software, San Diego, California USA	www.graphpad.com
Other		
Culture Medium RPMI 1640	Gibco	Cat#31870-025
Culture Medium DMEM	Gibco	Cat#21969-035
DMEM- high glucose, HEPES, no phenol red	Gibco	Cat#21063-029
Opti-MEM™ I Reduced Serum Medium, no phenol red	Gibco	Cat#11058-021
Fetal Bovine Serum	Gibco	Cat#10500-064
Penicillin-Streptomycin (5,000 U/mL)	Gibco	Cat# 15070-063
L-Glutamine (200 mM)	Gibco	Cat#25030-024

RESOURCE AVAILABILITY

Lead contact

Further information and requests for resources and reagents should be directed to and will be fulfilled by the Lead Contact, Maria M Mota (mmota@medicina.ulisboa.pt).

Materials availability

Plasmodium berghei uis4- (*Pbuis4-*) recombinant parasite and the *Pbuis4*-generation plasmid (p*Pbuis4-*) generated in this study are available upon request.

Data and code availability

Mass Spectrometry Analysis raw data with Mascot Search Results have been deposited at Mendley Data and are publicly available as of the date of publication. The DOI is listed in the Key resources table. Microscopy data, including all videos, reported in this paper will be shared by the Lead contact upon request.

This paper does not report original code.

Any additional information required to reanalyze the data reported in this paper is available from the Lead contact upon request.

EXPERIMENTAL MODEL AND SUBJECT DETAILS

Animal work

C57BL/6J and BALB/c WT mice (male, 6–8 weeks old) were purchased from the Charles River Breeding Laboratories and were housed in the Rodent Facility of Instituto de Medicina Molecular in Lisbon. All *in vivo* protocols were reviewed by iMM's Animal Welfare Body (ORBEA-iMM), and licensed by the national regulator, Direcção Geral de Alimentação e Veterinária (DGAV), and were performed according to national and European regulations.

Pbuis4⁻ parasite generation

Plasmodium berghei ANKA (*Pb*) *uis4* knockout line (*Pbuis4*⁻) was generated by the homologous recombination of the *Toxoplasma gondii* DHFR expression cassette (conferring resistance to Pyrimethamine) at the *uis4* ORF in a GFP expressing parasite line-507cl1 (Janse et al., 2006a). Primer sequences were used to amplify the 5′ and the 3′ untranslated regions (UTRs) of *Pbuis4* and, the *Pbuis4*⁻ plasmid vector was constructed for a double crossover homologous recombination, as previously described (Slavic et al., 2010). The final knockout construct was digested with *Kpn*I and *Not*I (New England Biolabs Inc.) to release the fragment for transfection. Transfection was performed using a protocol described elsewhere (Janse et al., 2006b). Briefly, blood from *Pb*WT infected BALB/c mouse was collected and cultured for 16 h *in vitro*. Mature schizonts were purified by a Nycodenz gradient and transfected using Amaxa electroporation system (Lonza). Transfected merozoites were injected into the tail vein of a BALB/c mouse and selected by the administration of Pyrimethamine in the drinking water (70 μg/mL). Pyrimethamine resistant parasite population containing the correct genomic integration of the *Pbuis4*⁻ construct were cloned by injecting one parasite per mouse (BALB/c).

Genotype and phenotype validation of the transgenic parasites

PCR analysis was performed on genomic DNA isolated from *Pbuis4*⁻ infected red blood cells (RBCs) to inspect if the transfection constructs integrated into the correct loci in Pyrimethamine-resistant parasites. DNA was isolated using the DNeasy Blood & Tissue Kit (QIAGEN). PCR was performed with the Nzytaq mastermix (Nzytech). The lack of *uis4* expression was further confirmed in transgenic parasites by RT-qPCR, immunofluorescence, and Western Blot.

Sporozoites purification

To obtain sporozoites for liver-stage experiments, *Anopheles stephensi* mosquitos (produced by Instituto de Medicina Molecular Insectary) were fed on BALB/c mice infected with either the *Pb*WT or *Pbuis4*⁻ parasites. For collection of salivary gland sporozoites, infected mosquitoes were dissected 21–35 days post-infection (d.p.i).

Mice infection

C57Bl/6J mice were intravenously injected with 50,000 *Pbuis4*⁻ or *Pb*WT sporozoites. At appropriate times livers were obtained and processed for subsequent analysis. In specific experiments, liver infection was allowed to progress to the blood stage of infection. The onset of blood parasitaemia was monitored from 2 days.p.i until 25 days.p.i by blood smear stained with Giemsa modified solution (Sigma-Aldrich).

Hepatoma cell line infection

Huh7 hepatoma cells (JCRB0403-NIBIOHN, Japan) were cultured in RPMI 1640 supplemented with 10% FBS, 50 μg per mL penicillin/streptomycin, 2 mM glutamine, 10 M HEPES and 10 mM Non-essential Amino acids (all Gibco), and, maintained in a 5% CO_2 humidified incubator at 37°C. 24 h prior to infection, 50,000

Huh7 cells were plated per well of a 24-well culture plate (Corning Costar). Cells were infected with 45,000 freshly dissected *Pb*WT or *Pbuis4*⁻ sporozoites per well by direct addition of sporozoites and centrifugation at 17.6*g* for 5 min 2 h.p.i, hepatoma cells were cultured in the presence of 0.3% v/v Fungizone (Gibco).

METHOD DETAILS

cDNA synthesis and real-Time PCR

Whole livers from infected mice were excised homogenized in 3 mL denaturing solution (4M guanidine thiocyanate; 25 mM sodium citrate pH 7; 0.5% N-Lauroylsarcosine and 0.7% β-Mercaptoethanol, in DEPC-treated water). RNA extraction was performed using the RNA extraction kit (Nzytech) from liver lysates, and with Purezol reagent (Bio-Rad) for infected Huh7 cells. 200-500 μg of RNA was reverse transcribed using the NZY First-Strand cDNA Synthesis Kit (Nzytech) as per manufacturer's instructions with the following conditions: 25°C, 10 min; 50°C, 50 min and 85°C, 5 min qRT-PCR was performed to detect *Pb18S* rRNA, *Pbuis4* and *Mmhprt* or *Hshprt* in the iTaq universal SYBR green supermix (Bio-Rad) using the 7,500 Fast qPCR system (Applied Biosystems). For analysis, the expression levels of targets were normalized against *hprt* housekeeping gene (ΔCt). Gene expression values were then calculated based on the ΔΔCt method, using the mean of the control group as the calibrator to which all other samples were compared.

Cell transfection

Human Embryonic Kidney 293T (HEK 293-T) cells and 3T3 fibroblast cells were cultured in DMEM supplemented with 10% FBS, 1% penicillin/streptomycin and 1% glutamine (all Gibco) and maintained in a 5% CO_2 humidified incubator at 37°C. For immunoprecipitation, five million HEK 293-T were seeded 24 h prior to transfection on a 10 cm cell culture dish in supplemented DMEM, without antibiotics. Cells were transfected with 5 μg of plasmids encoding *Pb*UIS4 or *Pb*UIS3. For actin structure analysis, 3T3 cells were separately transfected with 3 μg of codon optimized *Pb*UIS4 and *Pb*UIS3 expressing plasmids by reverse transfection and seeded on cover slips. All transfections were performed using FUGENE 6 (Promega) in a 3:1 ratio of transfection reagent to DNA and a day after transfection culture medium was replaced with fresh culture medium.

Immunoprecipitation

For immunoprecipitation of parasite-encoded UIS4 from infected cells, Huh7 cells were lysed 24 h post infection with *Pb*WT or *Pbuis4*⁻. Total cell lysates were collected in 0.5 mL lysis buffer (50 mM Tris-HCl pH 7.4, 0.5% NP-40, 250 mM NaCl, 5 mM EDTA, 50 mM NaF) supplemented with Complete protease inhibitor, PhosStop phosphatase inhibitor cocktail (Roche) and Phenylmethanesulfonylfluoride (Sigma). For HEK 293-T cells transiently expressing *Pb*UIS4 or *Pb*UIS3, collection was done 48 h after transfection and processed as described above. Total protein quantification of cell lysates was performed using the BCA Protein assay kit (Pierce™). Lysate pre-clearing was performed with 1.5 mg Protein-G beads for 1 h at 4°C followed by the magnetic removal of the same. UIS4 was immunoprecipitated from pre-cleared total cell lysates with anti-UIS4 antibody (incubated overnight at 4°C with rotation). Protein-G beads were employed to capture the antigen-antibody complex and removed magnetically to separate the immunoprecipitated fraction. The bound fraction was eluted from beads with 30μL of glycine (50 mM, pH 2.8), and the elute was equilibrated with 1.5μL of 1M Tris-HCl (pH10.02). The elute containing co-immunoprecipitated proteins were analysed by western blot with total cell lysates as control.

Western blot

Proteins were resolved on a denaturing (SDS) poly-acrylamide gel (5% stacking gel and 10% resolving gel) and electro-transferred to a nitrocellulose membrane. After washing, membranes were blocked in 5% non-fat dried milk (Molico Nestle™) solution in 0.2% Tween 20 - PBS (PBST) for 1 h at room temperature. Membranes were probed with anti-UIS4, anti-actin or anti-myc antibodies to detect UIS4, actin, and UIS3-myc respectively, followed by incubation in HRP-conjugated secondary antibodies (Jackson Immuno Research Laboratories). Immunoblots were developed using Luminata Crescendo Western HRP substrate reagent (Merck Millipore) and imaged with the ChemiDoc XRS system.

Silver staining

Silver staining was performed according the manufacturer's protocol (Silver Stain Kit, Thermo Scientific and PROTSIL, Sigma). Briefly, proteins were resolved on a 10% SDS-poly-acrylamide gel, the gel was washed

twice in ultrapure water (5 min) and fixed with 30% ethanol:10% acetic acid solution (15 min). After fixation, the gel was washed once in 30% ethanol (10 min) and twice in ultrapure water (5 min). Sensitization was performed in Silver Stain Sensitizer solution for 10 min and washed twice in ultrapure water (10 min). Finally, the gel was stained with Silver Stain solution for 30 min. Development with Silver Stain Developer solution was preceded by a 90 s wash in ultrapure water and stopped, when reaching the desired band intensity, with 5% acetic acid (10 min). At the end, the differentially expressed bands observed in *Pb*WT infected cells with respect to *Pbuis4⁻* infected cells, were excised from the gel and processed for mass spectrometry analysis. The corresponding molecular weight fractions on the *Pbuis4⁻* infected cells were excised as the control sample for analysis.

Mass spectrometry analysis

The mass spectrometry analysis was performed by UniMS- Mass Spectrometry Unit at ITQB/IBET (Instituto de Tecnologia Química e Biologica/Instituto de Biologia Experimental e Tecnológica, Portugal). Protein bands excised from a 1D-PAGE gel, were destained, reduced, alkylated, and digested with trypsin (Promega) overnight at 37ºC (6.7 ng/μL). The tryptic peptides were actively extracted from the bands, desalted, and concentrated using POROS R2 (Applied Biosystems) and, eluted directly onto the MALDI plate using 0.6 μL of 2.5 mg/mL CHCA (alpha-cyano-4-hydroxycinnamic acid, Sigma) in 50% (v/v) acetonitrile and 5% (v/v) formic acid. Data acquisition was performed on positive reflector MS and MS/MS modes using a 4800plus MALDI-TOF/TOF (ABSciex) mass spectrometer and using 4000 Series Explorer Software v.3.5.3 (Applied Biosystems). External calibration was performed using CalMix5 (Protea). The twenty-five most intense precursor ions from the MS spectra were selected for MS/MS analysis. The raw MS and MS/MS data were analyzed using the Protein Pilot Software v. 4.5 (ABSciex) with the Mascot search engine (MOWSE algorithm). The search parameters were as follows: monoisotopic peptide mass values were considered, maximum precursor mass tolerance (MS) of 50 ppm and a maximum fragment mass tolerance (MS/MS) of 0.3 Da. The search was performed against the SwissProt protein database with no taxonomic restriction. A maximum of two missed cleavages was allowed. Carboxyamidomethylation of Cysteines, oxidation of methionine and N-Pyro Glu of the N-terminal Q were set as variable modifications. Protein identification was only accepted when significant protein homology scores were obtained ($p < 0.05$, scores higher than 70) and at least one peptide was fragmented with a significant individual ion score ($p < 0.05$).

Blebbistatin treatment

Huh7 cells infected with *Pb*WT or *Pbuis4⁻* sporozoites were treated with 50 μM blebbistatin (Bio Vision) for 6 h starting at 24 h.p.i. At the end of treatment, the compound was washed out and cells were incubated with phenol red free DMEM (supplemented with 10% FBS and 1% Glutamine) for live imaging experiments or re-incubated with fresh medium until 48 h.p.i. and processed for immunofluorescence analysis.

Immunofluorescence assay

Infected cells were fixed with 4% paraformaldehyde (PFA) in PBS (Nzytech) for 15 min at room temperature. Fixed cells were permeabilized with 0.2% Saponin (Sigma) in PBS containing 2% BSA (Nzytech), for 30 min at room temperature. Transfected cells were fixed with 4% PFA at room temperature for 10 min, permeabilized with 0.3% Triton X-100 in PBS for 5 min and blocked with 5% BSA in PBS for 1 h at room temperature. For immunostaining, coverslips were incubated with primary antibodies diluted in blocking solution (2 h, room temperature), washed with PBS, incubated for 1 h at room temperature with Alexa fluor-conjugated secondary antibodies (Molecular probes, Invitrogen, Thermo Scientific) and Hoechst 33342 (Invitrogen) and washed again. The coverslips were mounted on microscope slides with Fluoromount G (Invitrogen). For infection quantification by microscopy, parasites were stained with anti-*Pb*HSP70(Tsuji et al., 1994) or anti-GFP Alexa fluor-488 conjugate (Invitrogen) and imaged on a wide-field microscope equipped with an automated stage (Zeiss Axio observer, 40x Air (0.75), EC Plan-NeoFluar, Axiocam 506 mono-CCD (4.54*4.54 μm pixel size)). High-resolution images were acquired on point scanning confocal microscopes (Zeiss LSM 880 or LSM 710, 63x Oil (1.04) Plan-Apochromat DIC). All images were processed and analysed using ImageJ/FIJI (Schindelin et al., 2012).

Live imaging experiments and image analysis

Huh7 cells were reverse-transfected with mCherry-LifeAct expressing vector (gift from Michael Davidson, Addgene, 54491) and seeded on 35 mm μ-Dish (ibidi, GmbH) 24 h before infection. Infection was performed with 100,000 *Pb*WT or *Pbuis4⁻* sporozoites. Time-lapse imaging started at 24 h.p.i. on the Zeiss

CellPress
OPEN ACCESS

Axio-Observer (Spinning-disk confocal mode -Yokogawa CSU-X1 confocal scanner unit) with 63x magnification (Zeiss Objective Plan-Apochromat 63×/1.4 Oil DIC M27) in a micro-chamber (37°C and 5% humidified CO_2). Stack (z = 50) acquisition was performed over a period of a minimum of 6 h with an interval of 5 min. Excitation and detection settings for GFP and mCherry fluorescence was provided on Zen 2.6 (blue edition) (Excitation BP450–490 nm, Dichroic 495, emission 500–550; excitation 538–562 nm, Dichroic 570, emission 570–640, respectively, and Lasers: 488 (green) = 0.3%; 568 (mCherry) = 1.5%). For rescue experiments, imaging was performed starting at 30 h.p.i, (cells pre-treated with 50 μM Blebbistatin for 6 h), with the same acquisition settings except for the imaging interval (10 min). Videographic analysis was performed on Imaris (version 9.5, Oxford Instruments) with the inclusion criteria of live host cells throughout acquisition only. Events comprising of parasite GFP signal loss followed by closure of infection site were categorized in disappearance events. However, parasite signal loss in the absence of wound closure was not considered for actin driven parasite removal.

QUANTIFICATION AND STATISTICAL ANALYSIS

Data are expressed as means $\pm$ SE of mean (SEM). Statistically significant differences between two different groups were determined using non-parametric two-tailed-Mann-Whitney test, unpaired two-tailed t test, or two-way ANOVA, as indicated. p values < 0.05 were considered statistically significant. Significances are represented in the figures as follows: n.s. $p > 0.05$; *$p < 0.05$; **$p < 0.01$; ***$p < 0.001$; ****$p < 0.0001$. Statistical analyses were carried out on Prism v8.4.3 (GraphPad).